Available online at www.sciencedirect.com
ScienceDirect
European Journal of Medicinal Chemistry 43 (2008) 2395–2403
EUROPEAN JOURNAL OF MEDICINAL CHEMISTRY
http://www.elsevier.com/locate/ejmech

Original article

# Synthesis, anti-tubercular activity and 3D-QSAR study of coumarin-4-acetic acid benzylidene hydrazides

Atul Manvar [c], Alpeshkumar Malde [b], Jitender Verma [b], Vijay Virsodia [c], Arun Mishra [a], Kuldip Upadhyay [d], Hrishikesh Acharya [a], Evans Coutinho [b,**], Anamik Shah [c,*]

[a] *Jubilant Organosys, 1A, Sector 16A, Noida 201 301, Uttar Pradesh, India*
[b] *Department of Pharmaceutical Chemistry, Bombay College of Pharmacy, Kalina, Santacruz (E), Mumbai 400 098, India*
[c] *Department of Chemistry, Saurashtra University, University Road, University Campus, Rajkot 360 005, Gujarat, India*
[d] *Torrent Research Centre, Bhat, Gandhinagar, India*

Received 24 May 2007; received in revised form 3 January 2008; accepted 3 January 2008
Available online 29 January 2008

**Abstract**

A set of 25 coumarin-4-acetic acid benzylidene hydrazides were synthesized and characterized by NMR, IR and mass spectroscopic techniques. The compounds were evaluated for their anti-tubercular activity against *Mycobacterium tuberculosis* $H_{37}Rv$ strain using the BACTEC 460 system to determine percentage inhibition. To understand the relationship between structure and activity, a 3D-QSAR analysis has been carried out by Comparative Molecular Field Analysis (CoMFA). Several statistically significant CoMFA models were generated. The CoMFA model generated with *database* alignment was the best in terms of overall statistics. The CoMFA contours provide a good insight into the structure activity relationships of the compounds reported herein.


*Keywords:* Coumarin-hydrazides; Anti-tubercular activity; CoMFA; 3D-QSAR study

## 1. Introduction

*Mycobacterium tuberculosis*, a human pathogen causing tuberculosis (TB), claims more human lives than any other bacterial pathogens [1,2]. It is estimated that 9 million new TB cases and approximately 2 million deaths occurred worldwide in the year 2004, and more that 80% of those were in developing countries [3]. According to WHO, from 2002 to 2020, there will be about 1 billion more people newly infected with TB and approximately 36 million deaths, if the worldwide ravage of tuberculosis is left unchecked [4]. As regards new drug development, not a single new anti-tubercular agent has been launched since the introduction of rifampicin in 1965, despite the great advances that have been made in drug discovery technologies [5]. The current WHO-approved treatment for TB, known as directly observed therapy short-course (DOTS), involves an intensive phase with three or four different drugs viz. isoniazid (INH), rifampin (RFP), pyrazinamide (PZA), and ethambutol (EB) for a minimum of 6 months [6]. INH, a well-known anti-tubercular drug, is believed to kill mycobacteria by inhibiting the biosynthesis of mycolic acids, critical components of the mycobacterial cell wall. The catalase and peroxidase activities are thought to participate in the drug sensitivity mechanism by converting INH *in vivo* into its biologically active form, which then act on its intracellular target [7]. In analogy to INH, pyridines substituted with alkylated tetrazoles (designed as lipophilic precursors of isosteres of isonicotinic acid) have been reported to possess anti-tubercular activity against the $H_{37}Rv$ strain of *M. tuberculosis*. These compounds, after penetration of the mycobacterial cell wall, are very likely biotransformed by esterases or peroxidase–catalases. They are more active than the unmodified polar isosteres of isonicotinic acid, which

* Corresponding author. Tel.: +91 281 2581013; fax: +91 281 2576802.
** Corresponding author. Tel.: +91 22 26670905.
*E-mail addresses:* evans@bcpindia.org, evans@bcp.edu.in (E. Coutinho), anamik_shah@yahoo.com, anamik_shah@hotmail.com (A. Shah).

0223-5234/$ - see front matter © 2008 Elsevier Masson SAS. All rights reserved.
doi:10.1016/j.ejmech.2008.01.016

may be due to better penetration of these agents into the cell wall of the mycobacteria [8].

The failure of patients to complete the therapy has led to the emergence of multidrug-resistant TB (MDR-TB), and multidrug-resistant (MDR) strains of *M. tuberculosis* that are resistant to the two major drugs isonicotinic acid hydrazide and rifampicin has further complicated the situation. The AIDS pandemic has led to an explosion of HIV/TB co-infection for patients living with HIV/AIDS. TB is a leading cause of death among people who are HIV-positive (13% of AIDS deaths worldwide). Consequently, there is a pressing need for the development of novel drugs for treating AIDS related TB that are effective against both drug-sensitive and drug-resistant MTB strains. The development of potent new anti-tubercular agents with low-toxicity profiles, effective against both drug-susceptible and drug-resistant strains of *M. tuberculosis* and capable of shortening the current duration of therapy are the need of the hour [9]. Recognizing these serious facts, we initiated a program to synthesize and screen diverse heterocyclic entities like quinolines and coumarins as anti-tubercular agents [10,11]. Among the heterocyclic group of compounds, naturally occurring derivatives of coumarin like Calanolide A show potent anti-tubercular activity with a MIC value of 3.13 μg/ml, and Calanolide B which is readily available from the *Calophyllum* seed, is claimed to have a comparable spectrum of activity as Calanolide A [12]. Inspired by this fact, we set upon a program of making anti-tubercular agents using the central coumarin ring in Calanolide A (structure A in Scheme 1) as the template and adding substituents as we deemed necessary to impart activity, on the various positions on the coumarin ring. As the first part of a series of coumarin analogs, we report here work on coumarin-4-acetic acid benzylidene hydrazides as anti-tubercular agents (structure B in Scheme 1). To probe the relationship between structure and activity for this class of compounds, Comparative Molecular Field Analysis (CoMFA) was also carried out.

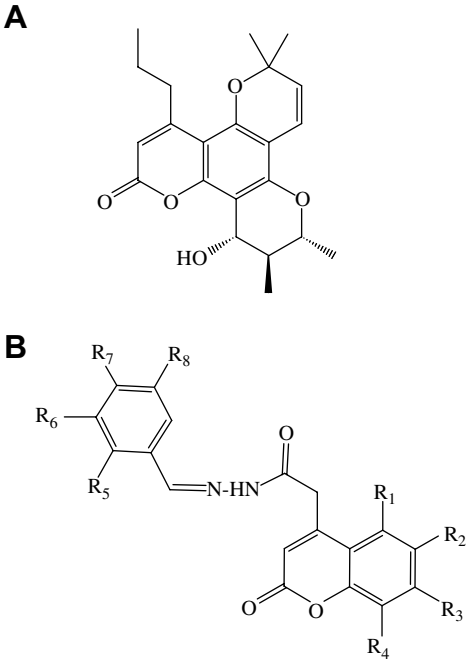


Scheme 1.

## 2. Results and discussion

### 2.1. Chemistry

The synthetic route employed to produce the series of 25 compounds **5**(**a**–**y**) are portrayed in Scheme 2. Citric acid in the presence of sulphuric acid at low temperature (10 °C) yields acetone dicarboxylic acid, which was not isolated, but directly reacted with phenol (**1**) to produce coumarin-4-acetic acid (**2**) under Pechmann reaction conditions [13]. In the second step, esterification of coumarin-4-acetic acid was carried out with methanol in presence of an acid catalyst (**3**). Coumarin-4-acetic acid hydrazide (**4**) was synthesized by refluxing coumarin-4-acetic acid methyl ester with hydrazine hydrate. Final reflux with aldehyde in alcohol leads to the coumarin-4-acetic acid benzylidene hydrazides (**5a**–**y**).

### 2.2. Biology

All synthesized compounds were screened for anti-tubercular activity against *M. tuberculosis* $H_{37}Rv$ using rifampicin as the standard. MIC values were determined by the protocol discussed in Section 4.2, and the percentage inhibition was found to lie in a large range of 6–93%. It is important to note that the 7-hydroxycoumarin derivative with $R_6$=$NO_2$ (Table 2) shows the highest anti-TB activity, while introduction of methyl groups at $R_1$ and $R_4$ gives the second most potent compound. The dimethyl derivatives with nitro (**5f**) and chloro (**5c**) groups at $R_6$ show anti-TB activity with 65 and 62% inhibition, respectively. The effect of the electron donating methyl group on the coumarin skeleton along with electron withdrawing groups on the phenyl hydrazide moiety, on the activity, makes an interesting observation.

### 2.3. CoMFA studies

The geometry of the groups at the 4-position of the coumarin ring was adopted from the X-ray structure of a related molecule (*vide supra*). Various CoMFA[14] models were generated for two alignments, namely *database* and *field fit*, by varying the grid size and orientation of the aligned molecules in the grid. Only the two best models are reported here; model 1 obtained by *database* alignment and model 2 derived from *field fit* alignment. The statistics of these models are shown in Table 3. The activities of molecules **5d** and **5j** in the test set were poorly predicted by both models. The inclusion of these molecules in the test set decreased the value of $r^2_{cv}$ significantly. Hence, these molecules were considered as outliers and not included in the calculation of the predictive correlation coefficient ($r^2_{pred}$).

The two best models have parameters, which are statistically significant. Model 1 has overall better statistical qualities – a conventional correlation coefficient ($r^2$) of 0.983, a cross-validated correlation coefficient ($q^2$) of 0.636, and a predictive

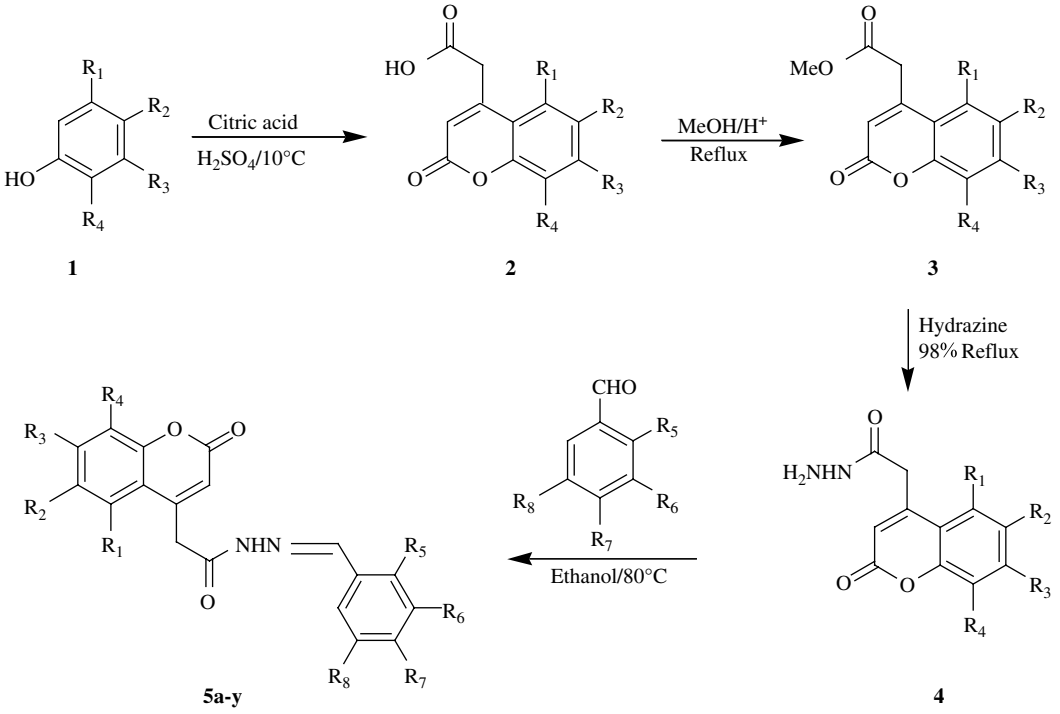


Scheme 2.

correlation coefficient ($r^2_{pred}$) of 0.338. Although the model obtained by *field fit* alignment exhibits higher $r^2_{pred}$ (0.464), the values of $r^2$ and $r^2_{cv}$ are relatively lower. Plots of the predicted *vs*. experimental activity of the training set molecules for models 1 and 2 are shown in Fig. 2.

The CoMFA model, with its hundreds or thousands of terms, is generally represented as a 3D 'coefficient contour'. Colored contours in the map represent those areas in 3D space where changes in the steric and electrostatic field values of a compound correlate strongly with concomitant change in its biological activity. The CoMFA steric and electrostatic contour plots of the best models are shown in Figs. 3 and 4, respectively.

Analysis of the steric contours of model 1 (Fig. 3A) reveals large green colored contours surrounding almost all the positions of the phenyl ring of the benzylidene hydrazide moiety. No yellow colored contours are visible, neither are any significant steric contours seen around the coumarin ring. The steric contours of model 2 (Fig. 3B) also lead to the same interpretation. The molecules with medium size substituents, for *e.g.* methoxy group, on the phenyl ring exhibit good inhibitory activity. For this very reason, molecules **5h** and **5u** with a tris–methoxyphenyl, molecule **5e** with *o*-methoxyphenyl, molecule **5r** with *p*-methoxyphenyl and molecule **5v** with *m,p*-dimethoxyphenyl moieties have high inhibitory activities.

Analysis of the electrostatic contours of model 1 (Fig. 4A) reveals blue colored contours near the *meta*- and *para*-positions of the phenyl ring of the benzylidene hydrazide moiety. Also there are two medium-sized blue colored contours away from the *ortho*-position of the phenyl ring. No electrostatic contours are seen around the coumarin ring. The electrostatic contours of model 2 (Fig. 4B) advocate almost similar requirements for activity as far as the benzylidene hydrazide moiety is concerned. In addition, there is also a big blue colored contour in the vicinity of the C6 and C7 positions, and a red colored contour close to the C7 and C8 positions of the coumarin ring. The highly active molecule (**5y**) in the series possesses an electronegative –OH substituent at the C7 position of the coumarin ring, which is near the favored red colored contour, leading to good activity. Molecules with a C6 methyl substituent (**5n–5x**) exhibit moderate to good inhibitory activity as the methyl group is near the electropositive favorable blue colored contour. Molecules **5j–5n** also have a C6 methyl substituent, but these have low activity as the additional C7 methyl substituent is near the disfavored red colored contour, which contributes to the reduction in their activity. Molecules with a *methoxy* substituent (**5e**, **5h**, **5r**, **5u**, **5v**) in the phenyl ring of the benzylidene hydrazide moiety have their methyl portion buried inside the favorable blue colored contour and thus exhibit good inhibitory activity. These blue colored contours partially overlap with the sterically favorable green colored contour around the phenyl ring.

## 3. Conclusions

Coumarin-4-acetic acid benzylidene hydrazides were synthesized in four convenient steps in *ca*. 60–70% yields. All compounds were tested for activity against *M. tuberculosis* $H_{37}Rv$ strain using rifampicin as the standard with the BACTEC 460 system to determine the percentage inhibition. A 3D-QSAR analysis of these compounds was carried out with CoMFA to map the structural features contributing to the inhibitory activity of these molecules. A number of models were generated based on *database* alignment as well as *field*

Table 1
Physical data of coumarin-4-acetic acid benzylidene hydrazides (**5a–y**)

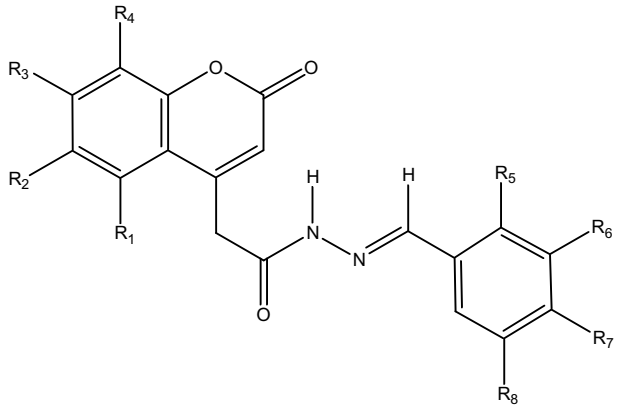


| No. | $R_1$ | $R_2$ | $R_3$ | $R_4$ | $R_5$ | $R_6$ | $R_7$ | $R_8$ | Mp °C | Yield % |
|---|---|---|---|---|---|---|---|---|---|---|
| **5a** | $CH_3$ | H | H | $CH_3$ | H | H | H | H | 174–176 | 62 |
| **5b** | $CH_3$ | H | H | $CH_3$ | Cl | H | H | H | 168–170 | 68 |
| **5c** | $CH_3$ | H | H | $CH_3$ | H | H | Cl | H | 157–159 | 67 |
| **5d** | $CH_3$ | H | H | $CH_3$ | H | H | $NMe_2$ | H | 163–165 | 59 |
| **5e** | $CH_3$ | H | H | $CH_3$ | OMe | H | H | H | 161–163 | 55 |
| **5f** | $CH_3$ | H | H | $CH_3$ | $NO_2$ | H | H | H | 175–177 | 69 |
| **5g** | $CH_3$ | H | H | $CH_3$ | H | $NO_2$ | H | H | 181–183 | 56 |
| **5h** | $CH_3$ | H | H | $CH_3$ | H | OMe | OMe | OMe | 185–187 | 61 |
| **5i** | H | $CH_3$ | $CH_3$ | H | Cl | H | H | H | 135–137 | 67 |
| **5j** | H | $CH_3$ | $CH_3$ | H | H | H | Cl | H | 178–179 | 60 |
| **5k** | H | $CH_3$ | $CH_3$ | H | H | H | SMe | H | 145–147 | 61 |
| **5l** | H | $CH_3$ | $CH_3$ | H | $NO_2$ | H | H | H | 165–167 | 69 |
| **5m** | H | $CH_3$ | $CH_3$ | H | H | $NO_2$ | H | H | 201–203 | 71 |
| **5n** | H | $CH_3$ | H | H | H | H | H | H | 189–191 | 59 |
| **5o** | H | $CH_3$ | H | H | Cl | H | H | H | 201–203 | 60 |
| **5p** | H | $CH_3$ | H | H | H | H | Cl | H | 195–197 | 64 |
| **5q** | H | $CH_3$ | H | H | H | $NO_2$ | H | H | 198–200 | 60 |
| **5r** | H | $CH_3$ | H | H | H | H | OMe | H | 150–152 | 55 |
| **5s** | H | $CH_3$ | H | H | H | H | F | H | 168–170 | 62 |
| **5t** | H | $CH_3$ | H | H | OH | H | H | H | 168–170 | 58 |
| **5u** | H | $CH_3$ | H | H | H | OMe | OMe | OMe | 178–180 | 57 |
| **5v** | H | $CH_3$ | H | H | H | OMe | OMe | H | 185–187 | 61 |
| **5w** | H | $CH_3$ | H | H | H | OMe | H | H | 184–186 | 61 |
| **5x** | H | $CH_3$ | H | H | H | Cl | H | H | 160–162 | 59 |
| **5y** | H | H | OH | H | H | $NO_2$ | H | H | 175–177 | 60 |

*fit* alignment methodologies. Of the various models evaluated, the CoMFA model derived from *database* alignment was the best with a good correlation and predictive power. Analysis of the CoMFA contours provides details on the fine relationship linking structure and activity, and provides clues for structural modifications that can improve the activity.

## 4. Experimental

### *4.1. Chemistry*

All the chemicals and solvents were purchased from Spectrochem, S D Fine Chemicals and Loba Chemie (India) and used without further purification. Melting points were determined in open capillary tubes with an Electrothermal-9200 melting point apparatus and are reported here as uncorrected values. $^1$H NMR spectra were recorded on Bruker Avance II 300 MHz spectrometer in DMSO-$d_6$. Chemical shifts ($\delta$) are given in ppm relative to TMS, coupling constants ($J$) in Hz. FAB-Mass spectra were recorded on Jeol SX 102/DA-6000 and IR spectra were recorded on a Shimadzu FTIR-8400 using KBr optics.

#### *4.1.1. Synthesis of substituted coumarin-4-acetic acid (**2**)*

It was synthesized according to the procedure reported in the literature [13]. Accordingly, a mixture of citric acid (1 mol) and conc. sulphuric acid (32 ml) was stirred for half an hour, then the temperature was slowly raised during an interval of 10–15 min and as soon as the evolution of gas slackened, the flask was removed form the bath, allowed to stand for 15 min till the reaction mixture became clear and free from carbon monoxide bubbles; this was then cooled to 10 °C. To this solution, substituted phenol (1 mol) was added at 10 °C, drop wise. After the addition of phenol, the reaction

Table 2
Anti-tubercular activity of coumarin-4-acetic acid benzylidene hydrazides (**5a–y**)

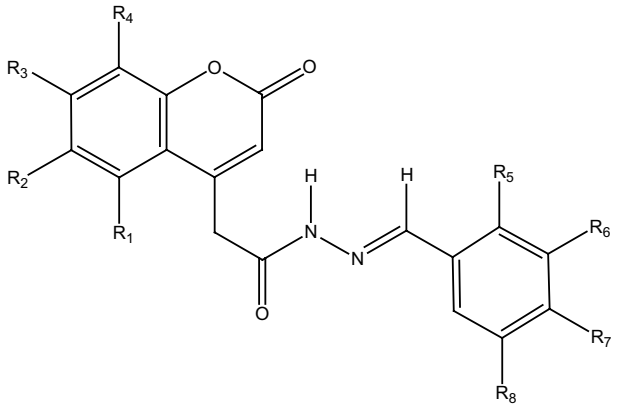


| No. | Conc. (μg/ml) | % Inhibition | logit Values |
|---|---|---|---|
| **5a** | 12.5 | 70 | 4.80 |
| **5b** | 12.5 | 48 | 4.44 |
| **5c** | 12.5 | 62 | 4.68 |
| **5d** | 12.5 | 7 | 3.36 |
| **5e** | 12.5 | 54 | 4.53 |
| **5f** | 12.5 | 65 | 4.75 |
| **5g** | 12.5 | 39 | 4.29 |
| **5h** | 12.5 | 52 | 4.57 |
| **5i** | 12.5 | 17 | 3.78 |
| **5j** | 12.5 | 32 | 4.14 |
| **5k** | 12.5 | 6 | 3.29 |
| **5l** | 12.5 | 11 | 3.57 |
| **5m** | 12.5 | 31 | 4.13 |
| **5n** | 6.25 | 34 | 4.42 |
| **5o** | 6.25 | 34 | 4.47 |
| **5p** | 6.25 | 19 | 4.12 |
| **5q** | 6.25 | 19 | 4.14 |
| **5r** | 6.25 | 33 | 4.44 |
| **5s** | 6.25 | 26 | 4.28 |
| **5t** | 6.25 | 55 | 4.85 |
| **5u** | 6.25 | 34 | 4.53 |
| **5v** | 6.25 | 29 | 4.40 |
| **5w** | 6.25 | 19 | 4.12 |
| **5x** | 6.25 | 21 | 4.18 |
| **5y** | 6.25 | 93 | 5.89 |

mixture was stirred at room temperature for 48 hr. The reaction mixture was then poured onto crushed ice; the separated solid was filtered and dissolved in saturated sodium bicarbonate solution which on acidification gave the title compounds (yield 55–70%).

*4.1.2. Synthesis of coumarin-4-methylacetate (**3**)*

The substituted coumarin-4-acetic acid (1 mol) was dissolved in methanol (100 ml), and a few drops of sulphuric acid were added. The resulting reaction mixture was refluxed for an appropriate time. After the completion of the reaction as indicated by TLC (ethylacetate:hexane:4:6), methanol was evaporated and the resulting reaction mixture extracted with ethyl acetate, washed with sodium bicarbonate, then with brine and dried over anhydrous sodium sulphate. The solvent was removed *in vacuo* to give the title compounds (yield 75–79%).

Table 3
A summary of the statistics of the 3D-QSAR models

| Parameter | *Database* alignment | *Field fit* alignment |
|---|---|---|
| | CoMFA model 1 | CoMFA model 2 |
| $N$ | 6 | 5 |
| $r^2$ | 0.983 | 0.951 |
| $r^2_{cv}$ | 0.636 | 0.403 |
| LGO (5) | 0.522 | 0.473 |
| $F$-value | 116 | 51 |
| $r^2_{pred}$ | 0.338 | 0.464 |
| $r^2_{bs}$ | 0.992 | 0.991 |
| SD | 0.052 | 0.056 |
| *Contributions (%)* | | |
| Steric | 59.5 | 53.1 |
| Electrostatic | 40.5 | 46.9 |

$N$ = optimum number of components, $r^2$ = conventional (non-cross-validated) correlation coefficient, $r^2_{cv}$ = cross-validated correlation coefficient using *SAMPLS*, LGO (5) = cross-validation correlation coefficient by Leave-Group-Out (in groups of 5), $F$-value = Fisher statistics, $r^2_{pred}$ = predictive (test molecules) correlation coefficient, $r^2_{bs}$ = correlation coefficient after 100 runs of bootstrapping analysis, and SD = standard deviation from 100 bootstrapping runs.

*4.1.3. Synthesis of coumarin-4-acetic acid hydrazides (**4**)*

A mixture of coumarin-4-acetic acid methyl ester (0.1 mol) and hydrazine hydrate 98% (0.5 mol) was refluxed for an appropriate time. The reaction was monitored by TLC (methanol: chloroform:0.5:9.5). After completion of the reaction as indicated by TLC, the reaction mixture was poured into water and the solid which separated filtered off. It was the recrystallized from ethanol to give the title compounds (yield 65–72%).

*4.1.4. General synthesis of 4-(substituted benzylidenacetohydrazide)-coumarin (**5a–y**)*

A mixture of coumarin-4-acetic acid hydrazides (0.01 mol) and aromatic aldehydes (0.01 mol) were refluxed in absolute alcohol for an appropriate time. The reaction was monitored by TLC (ethylacetate:hexane:8:2). After completion of the reaction as indicated by TLC, ethanol was evaporated, to give the crude title compounds. Finally purification was achieved on silica gel (100–200 mesh) column chromatography using ethyl acetate/hexane as the eluents.

*4.1.4.1. 4-(2′-methoxy benzylidenacetohydrazide)-5,8-dimethylcoumarin **5e**.* $^1$H NMR (DMSO-$d_6$) $\delta$ ppm: 2.21 (s, 3H, $-CH_3$), 2.24 (s, 3H, -$CH_3$), 3.24 (s, 3H, $-OCH_3$), 3.39–4.09 (m, 2H, $-CH_2$), 6.35 (d, 1H, −CH), 6.79 (q, $J = 9.7$, 1H, −CH), 7.22 (d, $J = 8.9$, 1H, Ar−H), 7.45 (d, $J = 8.8$, 1H, Ar−H), 7.49–7.70 (m, 3H, Ar−H); $^{13}$C NMR ($\delta$): 171.5, 161.5, 159.2, 156.4, 150.9, 144.2, 134.5, 133.9, 133.1, 130.2, 129.3, 128.6, 125.1, 122.3, 117.5, 114.9, 112.9, 56.2, 44.9, 19.1, 14.8; IR (KBr): cm$^{-1}$ 3079 (=C−H), 2970 (C−H as), 2865 (C−H sy), 1695 (C=N), 1687 (C=O, amide), 1717 (C=O, lactone), 1644 (C=C), 1254 (C−O); FAB Mass: *m/z* 364 ($M^+$).

*4.1.4.2. 4-(4′-thiomethoxy benzylidenacetohydrazide)-6,7-dimethylcoumarin **5k**.* $^1$H NMR (DMSO-$d_6$) $\delta$ ppm: 2.29 (s, 3H, $-CH_3$), 2.32 (s, 3H, $-CH_3$), 2.47 (s, 3H, $-SCH_3$)

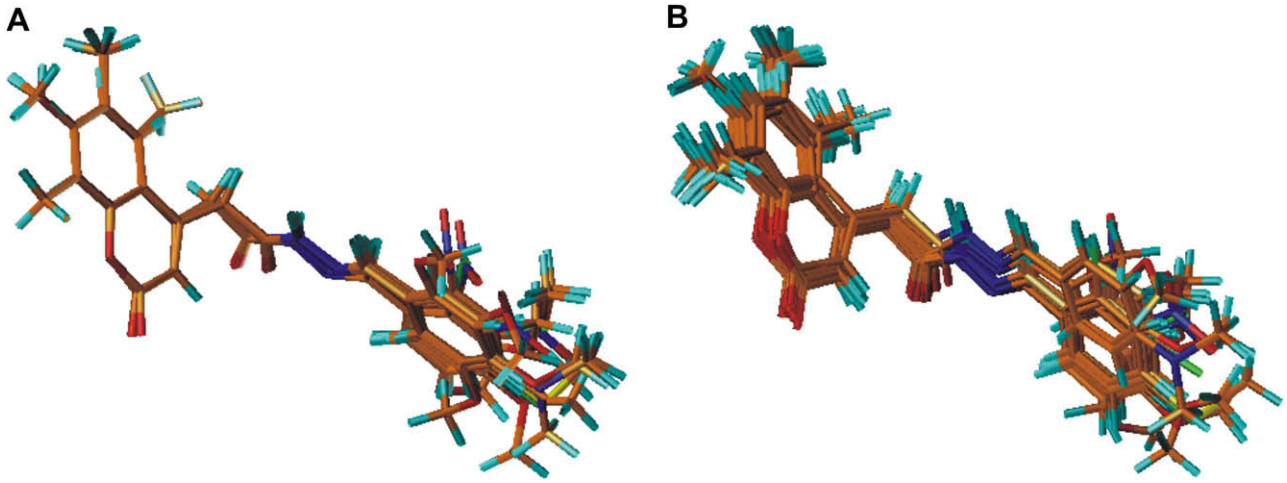


Fig. 1. A view of the molecules aligned using (A) *database* and (B) *field fit* alignment strategies.

3.41–4.13 (m, 2H, $-CH_2$), 6.29 (d, 1H, −CH), 6.79 (q, $J = 9.2$, 1H, −CH), 7.75 (s, 1H, Ar−H), 7.29 (s, 1H, Ar−H), 7.67 (m, 3H, Ar−H); $^{13}$C NMR ($\delta$): 171.9, 161.7, 155.4, 147.7, 144.2, 139.2, 137.1, 134.2, 130.7, 129.9, 127.3, 127.0, 120.9, 118.5, 113.2, 45.9, 18.8, 17.9, 15.2; IR (KBr): $cm^{-1}$ 3087 (=C−H), 2960 (C−H as), 2872 (C−H sy), 1690 (C=N), 1680 (C=O, amide), 1719 (C=O, lactone), 1652 (C=C), 795 (C−S); FAB Mass: *m/z* 380 ($M^+$).

*4.1.4.3. 4-(benzylidenacetohydrazide)-6-methylcoumarin* ***5n***. $^1$H NMR (DMSO-$d_6$) $\delta$ ppm: 2.35 (s, 3H, $-CH_3$), 3.49–4.09 (m, 2H, $-CH_2$), 6.31 (d, 1H, −CH), 6.79 (q, $J = 10.1$, 1H, −CH), 7.81–7.21 (m, 8H, Ar−H); $^{13}$C NMR ($\delta$): 171.7, 161.3, 155.8, 147.5, 143.4, 135.3, 134.3, 131.5, 129.9, 129.4, 129.1, 127.5, 121.7, 121.0, 113.2, 46.2, 25.2; IR (KBr): $cm^{-1}$ 3070 (=C−H), 2977 (C−H as), 2875 (C−H sy), 1679 (C=N), 1681 (C=O, amide), 1724 (C=O, lactone), 1649 (C=C); FAB Mass: *m/z* 320 ($M^+$).

*4.1.4.4. 4-(4′-chloro benzylidenacetohydrazide)-6-methylcoumarin* ***5p***. $^1$H NMR (DMSO-$d_6$) $\delta$ ppm: 2.30 (s, 3H, $-CH_3$), 3.47–4.19 (m, 2H, $-CH_2$), 6.37 (d, 1H, −CH), 6.85 (q, $J = 10.8$, 1H, −CH), 7.81–7.12 (m, 6H, Ar−H); $^{13}$C NMR ($\delta$): 172.1, 161.5, 155.7, 147.6, 144.2, 136.9, 135.6, 131.9, 131.2, 129.4, 129.1, 127.6, 122.0, 121.4, 112.8, 45.8, 24.8; IR (KBr): $cm^{-1}$ 3071 (=C−H), 2985 (C−H as), 2885 (C−H sy), 1684 (C=N), 1688 (C=O, amide), 1722 (C=O, lactone), 1639 (C=C), 790 (Ar−Cl); FAB Mass: *m/z* 355 ($M^+$).

*4.1.4.5. 4-(3′,4′-dimethoxy benzylidenacetohydrazide)-6-methylcoumarin* ***5v***. $^1$H NMR (DMSO-$d_6$) $\delta$ ppm: 2.30 (s, 3H, $-CH_3$), 3.19 (s, 3H, $-OCH_3$), 3.22 (s, 3H, $-OCH_3$) 3.41–4.11 (m, 2H, $-CH_2$), 6.39 (d, 1H, −CH), 6.81 (q, $J = 9.3$, 1H, −CH), 7.65–711 (m, 5H, Ar−H); $^{13}$C NMR ($\delta$): 171.8, 161.4, 155.3, 152.5, 150.2, 147.7, 143.9, 135.5, 129.0, 127.6, 127.2, 122.9, 121.9, 121.4, 115.9, 115.0, 112.7, 56.5, 56.2, 45.8, 25.0; IR (KBr): $cm^{-1}$ 3069 (=C−H), 2980 (C−H as), 2869 (C−H sy), 1685 (C=N), 1680 (C=O, amide), 1720 (C=, lactone), 1645 (C=C), 1260 (C−O); FAB Mass: *m/z* 379 ($M^+$).

*4.1.4.6. 4-(3′-methoxy benzylidenacetohydrazide)-6-methylcoumarin* ***5w***. $^1$H NMR (DMSO-$d_6$) $\delta$ ppm: 2.25 (s, 3H, $-CH_3$), 3.21 (s, 3H, $-OCH_3$), 3.39–4.19 (m, 2H, $-CH_2$), 6.50 (d, 1H,

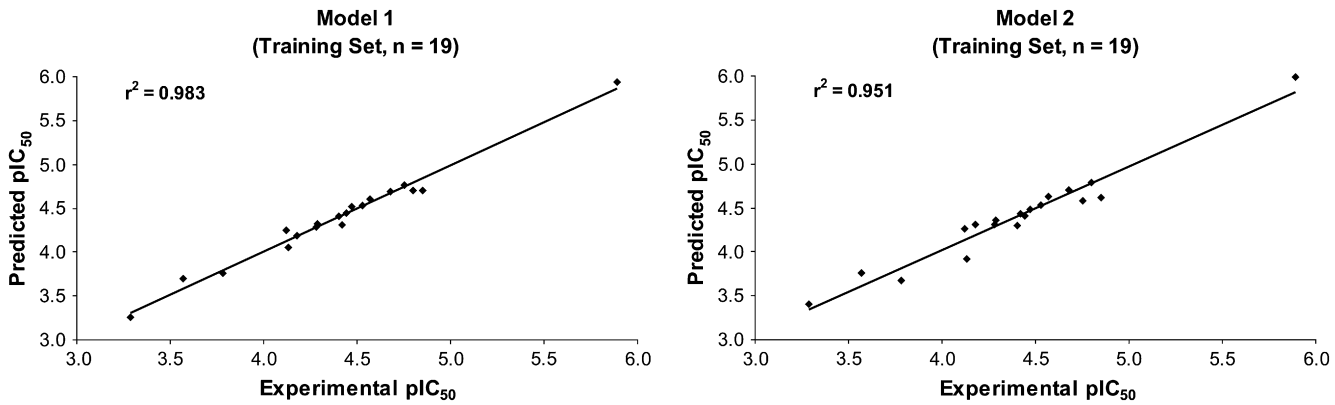


Fig. 2. Predicted *vs.* experimental activity for molecules in the training set based on models 1 and 2.

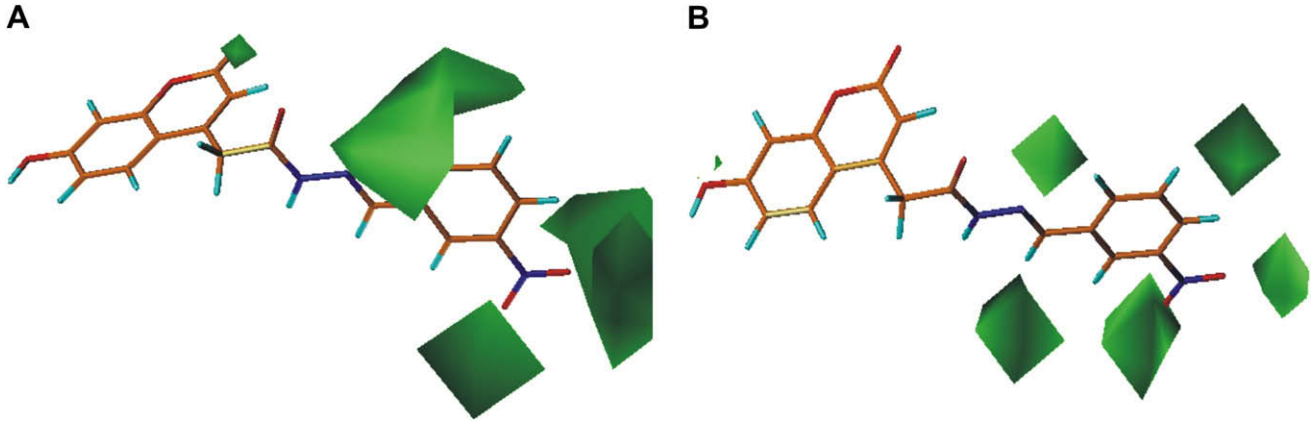


Fig. 3. CoMFA contours showing steric fields around molecule **5y** for (A) model 1 and (B) model 2. The green colored contour favors steric bulk, while sites where steric bulk is disfavored are shown in yellow [for interpretation of the references to color in this figure legend, the reader is referred to the web version of this article].

–CH), 6.77 (q, $J = 10.6$, 1H, –CH), 7.79–7.25 (m, 6H, Ar–H); $^{13}$C NMR ($\delta$): 171.3, 160.9, 161.4, 155.5, 147.8, 144.1, 135.7, 135.2, 130.4, 129.0, 127.5, 121.9, 121.7, 121.0, 117.2, 113.9, 112.8, 56.3, 45.7, 24.5; IR (KBr): cm$^{-1}$ 3070 (=C–H), 2987 (C–H as), 2875 (C–H sy), 1677 (C=N), 1689 (C=O, amide), 1712 (C=O, lactone), 1641 (C=C), 1269 (C–O); FAB Mass: *m/z* 350 ($M^+$).

### 4.2. Anti-tubercular activity

Anti-tubercular activity was determined using the modified BACTEC 460 system in which stock solutions as test compounds were prepared in dimethylsulfoxide (DMSO) at 1 mg/ml and sterilized by passage through 0.22 μm PFTE filters (Millex-FG, Millepore, Bedford, MA) 50 ml was added to 4 ml radiometric $7H_{12}$ broth (BACTEC-12B; Bectron Dickinson Diagnostic Instrument system, Sparks, MD) to achieve a final concentration of 12.5 μg/ml (**5a–m**) and 6.25 μg/ml (**5n–y**) (Table 2). Controls received 50 μL DMSO. Rifampin (Sigma Chemicals Co., St. Louis, MO) was included as a positive drug control. Rifampicin was solubilized and diluted in DMSO and added to BACTEC-12 broth to achieve a range of concentration for determination of minimum inhibitory concentration (MIC, lowest concentration inhibiting 99% of the inoculums, MIC value of rifampicin is 0.25 g/ml at 95% inhibition of $H_{37}$Rv strain). *M. tuberculosis* $H_{37}$Rv strain (ACTT 27294; American type culture collection, Rockville, MD) was cultured at 37 °C on a rotary shaker in middle brook $7H_9$ broth (Difco Laboratories, Detroit, MI) supplemented with 0.2 v/v glycerol and 0.05% v/v Tween 80, until the culture turbidity achieved an optical density of 0.45–0.55 at 550 nm. Bacteria were pelleted by centrifugation, washed twice and resuspended in one fifth of the original volume in Dulbecoo's phosphate buffered saline [PBS, Irvine Scientific, Santa Ana (A)]. Large bacterial clumps were removed by passage through an 8 μm filter (Malgene, Rochester, NY) and aliquots were frozen at −80 °C. Cultures were prepared and an appropriate dilution performed such that a BACTEC-12B vial inoculated with 0.1 ml would reach a growth index (GI) of 999 in 5 days. One tenth of the diluted inoculum was used to inoculate 4 ml of fresh BACTEC-12B broth containing the test compounds. An additional control vial was included which received a further 1:100 diluted inoculum (as well as 50 μL DMSO) for use in calculating the MIC of rifampicin, respectively, by established procedures. Cultures were incubated at 37 °C and the Growth of Inhibition (GI) determined daily until

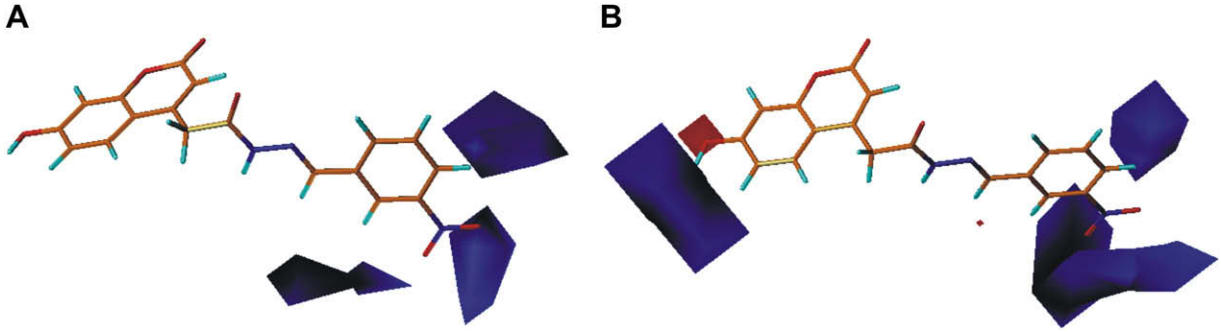


Fig. 4. CoMFA contours showing electrostatic fields around molecule **5y** for (A) model 1 and (B) model 2. The red contour shows regions where electronegative substituents are favored, while the blue contour is associated with positions where electropositive substituents improve activity [for interpretation of the references to color in this figure legend, the reader is referred to the web version of this article].

control cultures achieved a GI of 999. Assays were usually completed in 5–8 days. Percent inhibition was defined as 1-(GI of test sample/GI of control) × 100. Minimum inhibitory concentration of compound effecting a reduction in daily change in GI, which was less than that observed with a 1:100 diluted control culture on day the later reached a GI of at least 30.

### 4.3. Computational details

#### 4.3.1. Data set

A set of 25 molecules (Table 1) was used in the 3D-QSAR study. The data set was divided into a training set (19 molecules) and a test set (6 molecules: i.d.'s **5b**, **5d, 5j**, **5q**, **5u**, **5w**) by means of chemical as well as biological diversity. Daylight fingerprints of the molecules along with the $pIC_{50}$ data were used to separate the molecules into training and test sets based on the Tanimoto similarity coefficient [15].

#### 4.3.2. Biological data

For the QSAR study, the activity values were transformed as follows [16]:

$$\text{Activity} = -\log c + \text{logit}$$

where $c$ is the molar concentration = concentration (μg/ml) × 0.001/(molecular weight).

$$\text{logit} = \log[\%\ \text{inhibition}/(100 - \%\ \text{inhibition})]$$

#### 4.3.3. Molecular modeling

The CoMFA [14] studies were carried with *Sybyl 7.1* [17] installed on a Pentium 2.8 GHz PC running under the Linux OS (Red Hat Enterprise WS 2.3.1).

The coumarin ring, common to all molecules, is a rigid moiety. The orientation of the substituent at the 4th position of the coumarin ring was derived from a related crystal structure **cr1165** (Scheme 3) [18]. The geometry of the −CONHN=CH−Ph group was derived from the crystal structure of **bt2126** (Scheme 2). The structures of the molecules were built with the *Sketcher* module in *Sybyl* and energy minimized by *Powell's method* using the *MMFF94* force field [19] with a distance-dependent dielectric term.

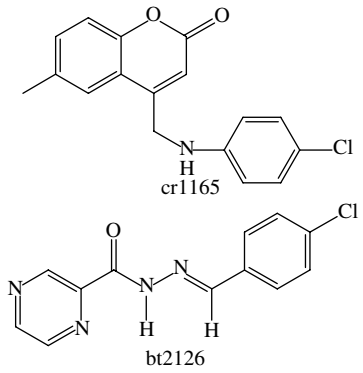


Scheme 3.

#### 4.3.4. Alignment

The most crucial input for the CoMFA is the alignment of the molecules. Molecule **5y** with the highest activity was chosen as the template and all other molecules were aligned to it using the *database* alignment method in *Sybyl* (Fig. 1A). The molecules were aligned with reference to the coumarin ring. A second alignment was also carried out using the *field fit* method, where the steric and electrostatic fields around the molecules were superimposed over the same fields of the template molecule (Fig. 1B).

#### 4.3.5. CoMFA interaction energy calculation

The steric and electrostatic fields in CoMFA were calculated using an $sp^3$ carbon atom with +1.0 charge as the probe. The van der Waals potential and Coulombic energy between the probe and the molecule were calculated using the standard Tripos force field. A distance-dependent dielectric constant of *1.0r* was used in the calculation of the electrostatics. The steric field was truncated at points where the value exceeded ±30.0 kcal/mol, and the electrostatic fields were ignored at those lattice points where the steric interactions were high. In order to investigate the effect of grid spacing, initially the CoMFA models were developed at varying grid spacing values (*i.e.* 0.5, 1.0, 1.5 and 2.0 Å). In both *database* as well as *field fit* alignment of molecules, the best $q^2$ values were obtained when the grid spacing was set to 2.0 Å which is the default grid spacing in *Sybyl*. Thus, further model development was done at a grid spacing of 2.0 Å.

Further, the influence of the overall orientation of the aligned molecules in the grid was examined by a protocol similar to that of Cho and Tropsha [20]. For this, starting from a random orientation, the entire aggregate of aligned molecules was rotated systematically in steps of 90° around the *x*, *y* and z-axes using the *STATIC ROTATE* command in *Sybyl*. For each orientation, the optimum number of components and $q^2$ values were obtained. The $q^2$ values varied from 0.165 to 0.636 for *database* alignment and from 0.108 to 0.403 for *field fit* alignment. The orientation of the aligned molecules with the best $q^2$ values was selected for further model development.

#### 4.3.6. Partial Least Squares (PLS) analysis

The PLS method was used to set up a correlation between the molecular fields and the inhibitory activity of the molecules. The optimal number of components was determined with *SAMPLS* (*Sam*ples-distance *P*artial *L*east *S*quare) [21] and cross-validation was carried out by the *leave-one-out* method. The model with the optimum number of components (highest $q^2$) and with the lowest standard error of prediction (SDEP) was considered for further analysis. Equal weights were assigned to the steric and electrostatic fields by the *COMFA_STD* scaling option. To speed up the analysis and reduce noise, columns with an $\sigma$ value below 2.0 kcal/mol were filtered off and the conventional $r^2$ was calculated using the optimum number of components. The final models were then refined by the *Region Focusing* [20] option in *Sybyl*, which concentrates only on those lattice points which are most pertinent to the model and thus enhances its resolution

and predictive power. To further assess the robustness and statistical confidence of the derived models, cross-validation by Leave-Group-Out[22] (LGO in groups of 5) and bootstrapping [22] analysis for 100 runs was performed. Bootstrapping involves the generation of many new data sets from the original data set and is obtained by randomly choosing samples from the original data set. The statistical calculation is performed on each of these bootstrap samplings. The difference between the parameters calculated from the original data set and the average of the parameters calculated from the many bootstrap samplings is a measure of the bias of the original calculations. Models with a cross-validation ($q^2$) value above 0.3 were sought, since at this value the probability of chance correlation is less than 5% [23].

#### 4.3.7. Predictive correlation coefficient

The predictive ability of each 3D-QSAR model was determined from a test set of 6 molecules not included in the model generation. The predictive correlation coefficient ($r^2_{\text{pred}}$), based on the test set molecules, is defined as

$$r^2_{\text{pred}} = (\text{SD} - \text{PRESS})/\text{SD}$$

where SD is the sum of squared deviations between the biological activity of the test set and the mean activity of the training set molecules and the PRESS is the sum of squared deviations between predicted and actual activity values for every molecule in the test set.

#### 4.3.8. CoMFA contour maps

Contour maps were generated as a scalar product of coefficients and standard deviation (SD × Coeff) associated with each column. Favored and disfavored levels, fixed at 80 and 20%, respectively, were used to display the steric and the electrostatic fields. The contours for steric fields are shown in green (more bulk favored) and yellow (less bulk favored), while the electrostatic field contours are displayed in red (electronegative substituents favored) and blue (electropositive substituents favored) colors.

## Acknowledgements

The authors are grateful to Department of Chemistry, Saurashtra University, Rajkot, India for providing necessary infrastructural facilities for carrying out synthetic work, and Dr. Cecil Kwong, TAACF, USA for anti-tubercular activity of the compounds. Atul Manvar is thankful to Department of Science and Technology (DST), India for the financial assistance. Alpeshkumar Malde and Jitender Verma thank the Council of Scientific and Industrial Research (CSIR), India for the award of a Senior Research Fellowship. The computational facilities at BCP were provided by the All India Council for Technical Education through grant F. No. 8022/RID/NPROJ/RPS-5/2003-04.

## References

[1] P.J. Dolin, M.D. Raviglione, Bull. World Health Organ. 72 (1994) 213–220.
[2] A.M. Rouchi, Chem. Eng. News 77 (1999) 52–69.
[3] Global Tuberculosis Control: Surveillance, Planning, Financing WHO Report, World Health Organization, Geneva, 2006, (WHO/HTM/TB/2006.362).
[4] WHO fact sheet Available from: http://www.who.int/mediacentre/factsheets/who104/en/print.html.
[5] W.J. Burman, B.E. Jones, Am. J. Respir. Crit. Care Med. 164 (2001) 7–12.
[6] R.V. Somu, H. Boshoff, C. Qiao, E.M. Bennett, C.E. Barry, C.C. Aldrich, J. Med. Chem. 49 (2006) 31–34.
[7] K. Johnsson, P.G. Schultz, J. Am. Chem. Soc. 116 (1994) 7425–7426.
[8] G.A. Wächter, M.C. Davis, A.R. Martin, S.G. Franzblau, J. Med. Chem. 41 (1998) 2436–2438.
[9] (a) S. Kaufman, J. Van Embden, Trends. Microbiol. 1 (1993) 2–5;
(b) B.R. Bloom, C.J. Murray, Science 257 (1992) 1055–1064;
(c) M.A. Fischl, G.L. Daikos, R.B. Uttamchandani, R.B. Poblete, J.N. Moreno, R.R. Reyes, A.M. Boota, L.M. Thompson, T.J. Cleary, S.A. Oldham, Ann. Intern. Med. 117 (1992) 184–190.
[10] N. Dodia, A. Shah, Ind. J. Heterocycl. Chem. 9 (1999) 139–142.
[11] N. Dodia, A. Shah, Ind. J. Heterocycl. Chem. 10 (2000) 69–70.
[12] A. Nayyar, R. Jain, Curr. Med. Chem. 12 (2005) 1873–1886.
[13] (a) V. Pechmann, Duisberg, Ber. Dtsch. Chem. Ges. 16 (1883) 2127;
(b) V. Pechmann, Kraft, Ber. Dtsch. Chem. Ges. 34 (1901) 421;
(c) B.B. Dey, J. Chem. Soc., Perkin Trans. 1 107 (1915) 1606–1651;
(d) D.J. Limaye, J. Indian Chem. Soc. 4 (1927) 159–161.
[14] R.D. Cramer, D.E. Patterson, J.D. Bunce, J. Am. Chem. Soc. 110 (1988) 5959–5967.
[15] E.J. Martin, J.M. Blaney, M.A. Siani, D.C. Spellmeyer, A.K. Wong, W.H. Moos, J. Med. Chem. 39 (1995) 1431–1436.
[16] CoMFA and QSAR Manual, Sybyl 7.1, Associates Inc., 1699 S Hanley Road, St. Louis, MO 631444, USA.
[17] Sybyl 7.1, Tripos Associates Inc., 1699 S Hanley Road, St. Louis, MO 631444, USA.
[18] (a) A. Jain, M.V. Kulkarni, N.C. Shivaprakash, Acta Crystallogr. C62 (1995) 2585–2586;
(b) Y. Cui-Cui, W. Li, X. Zhi-Yong, S. Xue-Fang, Acta Crystallogr. E62 (2006) o3274–o3275.
[19] T.A. Halgren, J. Am. Chem. Soc. 112 (1990) 4710–4723.
[20] Sung Jin Cho, Alexander Tropsha, J. Med. Chem. 38 (1995) 1060–1066.
[21] B.L. Bush, R.B. Nachbar, J. Comput.-Aided. Mol. Des. 7 (1993) 587–619.
[22] R.D. Cramer III, J.D. Bunce, D.E. Patterson, I.E. Frank, Quant. Struct. Act. Relat. 7 (1988) 18–25.
[23] M. Clark, R.D. Cramer, D.M. Jones, D.E. Patterson, P.E. Simeroth, Tetrahedron Comput. Methodol. 3 (1990) 47–59.